

# Concurrent Growth of Kirkendall Pores and Vapor–Solid–Solid Protuberances on Ni Wires During Mo Vapor-Phase Deposition

CONG WANG and DAVID C. DUNAND

During vapor-phase deposition at 1273 K (1000 °C), by pack cementation, of Mo onto 127- $\mu\text{m}$ -diameter Ni wires, two phenomena are observed to occur concurrently, leading to strong surface roughening: (i) the inward radial growth of Kirkendall pores below the wire surface and (ii) the outward growth from the wire surface of protuberances with sizes as large as 15  $\mu\text{m}$ . High-aspect-ratio Kirkendall pores as long as 21  $\mu\text{m}$  are created because of imbalanced interdiffusion between Mo and Ni. These pores in turn, by reducing the flow of Mo into the wires, may enhance the outward growth of Mo-rich protuberances, further roughening the wire surface. These protuberances have faceted tips as well as terraces and steps, indicating that their growth is governed by the vapor–solid–solid mechanism.

DOI: 10.1007/s11661-014-2587-4

© The Minerals, Metals & Materials Society and ASM International 2014

## I. INTRODUCTION

NI-MO alloys, owing to their remarkable resistance to corrosion and wear, have been studied extensively, as reviewed by Brooks *et al.*<sup>[1]</sup> Mo acts in Ni as a solid solution strengthener<sup>[2,3]</sup> or promotes the formation of intermetallic precipitates,<sup>[4]</sup> contingent on specific alloy compositional requirement and thermal–mechanical processing history. When Mo is coated onto Ni, the interdiffusion behavior between the two elements determines the formation of terminal phases, such as  $\alpha$ -Ni(Mo) solid solution, NiMo and Ni<sub>4</sub>Mo, and vacancies, leading to Kirkendall pores when the interdiffusion fluxes are imbalanced.<sup>[5–10]</sup> While current literature is concentrated primarily on solid-state reactions *via* diffusion in Mo-Ni couples, we are not aware of any studies focusing on vapor-phase deposition of Mo onto Ni with concurrent interdiffusion, which is the topic of the present study.

Pack cementation is a widely used vapor-phase deposition process which is used to deposit primarily Al on Ni-base substrates, but also elements such as Cr, Si, and Ti onto substrates such as ferritic stainless steels, low-alloy steels, and intermetallic compounds.<sup>[11–14]</sup> To our knowledge, there is only one report on Mo cementation, which was performed with Ti as a substrate at 1073 K to 1323 K (800 °C to 1050 °C), resulting in the formation of a Mo-rich diffusion layer.<sup>[15]</sup> In this process, NH<sub>4</sub>Cl reacts with Mo powders in a pack to form MoCl<sub>4</sub>, which is gaseous at the processing temperature and is transported to the Ti

substrate where it decomposes into Mo and Cl<sub>2</sub>. The chlorine molecule diffuses back to the pack where it further reacts with Mo, closing the transport loop. The Mo atoms on the substrate diffuse into its volume to form a solid solution and/or intermetallic phases. It is the purpose of this study to expand this Mo cementation process to Ni substrates.

Another deposition process relying on the gas phase is the vapor–liquid–solid (VLS) process, which is a widely used route for the formation of nanowires and whiskers.<sup>[16–18]</sup> Essential to the VLS method is an operating temperature enabling the creation of a eutectic or near-eutectic liquid droplet located at the nanowire tip which serves as the preferential site for absorbing the solute-containing vapor phase and as the reservoir for continuously rejecting the supersaturated solute atoms. Researchers have recently demonstrated that nanowires and/or whiskers may grow below the eutectic temperature without the presence of liquid phases in a vapor–solid–solid (VSS) mechanism which is explained by the size-dependent eutectic temperature depression hypothesis<sup>[19,20]</sup> or by the formation of catalyzing intermetallic phases.<sup>[21–25]</sup> However, prevailing studies on both VLS and VSS are mostly addressing nanowire and/or whiskers growth at the sub-micron and nanometric scale. We are not aware of reports on VLS or VSS features with supra-micron scales, as described in the present study.

A mechanism relevant to Mo-Ni interdiffusion is the Kirkendall effect, which stems from an imbalance of vacancy flow during interdiffusion. As far as the Mo-Ni systems concerned, Kirkendall pores are always formed on the Ni-rich side of the diffusion couple, as Mo is the slower diffuser.<sup>[7–9]</sup>

Here, we report on the unusual interplay between the Kirkendall effect and the VSS mechanism during the vapor-phase deposition of Mo onto Ni wires. We first describe the progressive growth of elongated, radially oriented Kirkendall pores in Ni wires as a result of the interdiffusion between Mo and Ni. We then report on the nucleation and growth of surface protuberances on

CONG WANG, formerly with the Department of Materials Science and Engineering, Northwestern University, Evanston, IL, is now Professor with the College of Materials and Metallurgy, Northeastern University, Shenyang 110819, P.R. China. Contact e-mail: wangc@smm.neu.edu.cn DAVID C. DUNAND, Professor, is with the Department of Materials Science and Engineering, Northwestern University.

Manuscript submitted July 16, 2014.

Article published online September 30, 2014

the Ni wires, which could be enhanced by the presence of subsurface Kirkendall pores impeding the diffusion into the volume of Mo atoms. By examining the features relevant to the growth mechanism (*e.g.*, the formation of intermetallic phases, the high eutectic temperature, the occurrence of growth terraces, steps, and tip facets), we propose that these surface protuberances are created by the VSS mechanism. The unusual combination of the Kirkendall effect creating deep grooves into the surface of the Ni wires and the VSS mechanism creating outgrowth on the wire surface results in extreme surface roughening of the Ni wires when pack-cemented with a Mo-rich layer. This is pertinent to create Mo-rich surface layers on nickel and Ni-base superalloys suitable for harsh environment applications.

## II. EXPERIMENTAL PROCEDURES

### A. Molybdenum Pack Cementation

Raw materials employed in this study include commercial Ni wires (with a diameter of 127  $\mu\text{m}$ , 99.95 pct pure Ni, strand-annealed at 823 K (550 °C) for 1.2 second and rapidly cooled in hydrogen) from MWS Wire Industries and powders from Alfa Aesar (with particle size in parentheses):  $\text{Al}_2\text{O}_3$  (20 to 50  $\mu\text{m}$ ),  $\text{NH}_4\text{Cl}$  (100  $\mu\text{m}$ ), and Mo (2 to 7  $\mu\text{m}$ ).

Powders were mixed for 1 hour in a tumbler at the ratio of 3 wt pct  $\text{NH}_4\text{Cl}$ , 40 wt pct Mo, and 57 wt pct  $\text{Al}_2\text{O}_3$ . Twenty Ni wires, approximately 30 mm in length, were pack-cemented within a 30 g pack in a tube furnace under continuous argon flow at 1273 K (1000 °C). Detailed procedures can be found elsewhere.<sup>[26]</sup> Cementation was interrupted, and Ni wires were transferred from the spent pack and to a replenished pack after 2, 4, and 8 hours, with the last pack staying in the furnace for an additional 16 hours (total 24 hours).

### B. Microstructure Characterization

After removing from the pack, Ni wires were ultrasonically cleaned in acetone for 1 hour. Cross-sectional specimens were mounted in epoxy, then ground, and polished down to 0.05  $\mu\text{m}$  colloidal alumina by standard metallographic procedures. The microstructure was investigated by a Hitachi SU8030 scanning electron microscope (SEM) at an acceleration voltage of 15 kV. Compositional analysis was completed by the energy dispersive X-ray spectrometer (EDS) coupled to the SEM. EDS signal was calibrated by standard samples of pure Ni.

## III. RESULTS AND DISCUSSION

Cross-sectional views of polished wires after 2, 4, 8, and 24 hours Mo pack cementation are shown in Figures 1(a) through (d). With increasing deposition time, two salient features develop: (i) progressively directional growth of Kirkendall pores, and (ii) increasing density of peripheral protuberance. These are discussed in turns in the next two sections.

### A. Kirkendall Effect

Figure 1(a) illustrates that, after 2 hours vapor-phase deposition, Kirkendall pores are formed in limited quantity just under the surface of the wire, and that their sizes are in the range of 2 to 7  $\mu\text{m}$ . With prolonged Mo deposition, Kirkendall pores appear to grow in a directional manner. Pores are elongated in the radial direction and are separated from each other by spoke-like structures (as seen in cross-sections), and their length nearly doubles from an average of 13 to 21  $\mu\text{m}$  after 8- and 24-hours heat treatments, respectively. On cross sections (Figures 1(a) through (d)), some of the pores appear unconnected to the wire surface, while others are open to the surface. An elemental line scan shown in Figure 1(b) shows clearly that the Mo content decreases from a high value (4 at. pct) at the wire surface to essentially zero at the inner tips of the radial pores, confirming that the interdiffusion layer, with an average Mo content of about 2 at. pct, is as wide as the pore length. If the Mo-deposited wires were fully homogenized by interdiffusion, the final Mo in the Ni wire matrix is calculated to be ~0.7 at. pct.

The Kirkendall effect, which is observed in many metallic systems, is due to imbalanced interdiffusion, in the present case between Ni and Mo. The fact that pores are generated within the original wire volume indicates that Ni diffuses radially outwards more rapidly than Mo, in the deposited surface coating, does inwards, thus creating an outward net flux of Ni atoms, leaving vacancies in the Ni matrix. The interdiffusion coefficient  $D$ —estimated from  $D = x^2/t$  where  $x = 21 \mu\text{m}$  (the width of diffusion zone) and  $t = 24$  hours—is  $5.1 \times 10^{-15} \text{ m}^2/\text{s}$ , which is about 5 times the highest value reported in Ni-Mo interdiffusion couples at a somewhat higher temperatures 1323 K *vs* 1273 K (1050 °C *vs* 1000 °C).<sup>[9]</sup> The elongated pores leaving only thin metallic “spokes” connecting the Mo-rich coating to the bulk of the Ni wire may significantly reduce the capacity to transport Mo and Ni; so these diffusivity values are probably depressed compared to the true interdiffusion coefficient. Alternatively, the interdiffusion could be accelerated by the exothermic formation of NiMo phases.<sup>[27]</sup>

The Kirkendall effect has been reported in the Ni-Mo,<sup>[5,8]</sup> Ni-Mo-Cu,<sup>[9]</sup> and Ni-Mo-Co<sup>[7]</sup> systems. However, the directional growth of Kirkendall pores visible in Figures 1(a) through (d) is not reported in these articles, and is rarely known to occur in other metallic systems. Kirkendall pores with high aspect ratios and large sizes have been documented in Cu-NiAl and Ag-Au systems where they developed from an initial lens-like morphology to elongated or even necked shape along grain boundaries<sup>[28–30]</sup> and were explained by the “grain boundary Kirkendall effect” as a result of atomic (or vacancy) fluxes and pore formation at grain boundaries. It is unlikely that this effect can explain the radially oriented, elongated pores in the current Ni-Mo system since (i) the grain boundaries are not aligned radially in the Ni wires, unlike the Kirkendall pores and (ii) the initial average grain size of the Ni wires (13  $\mu\text{m}$ , as measured metallographically) is larger than the

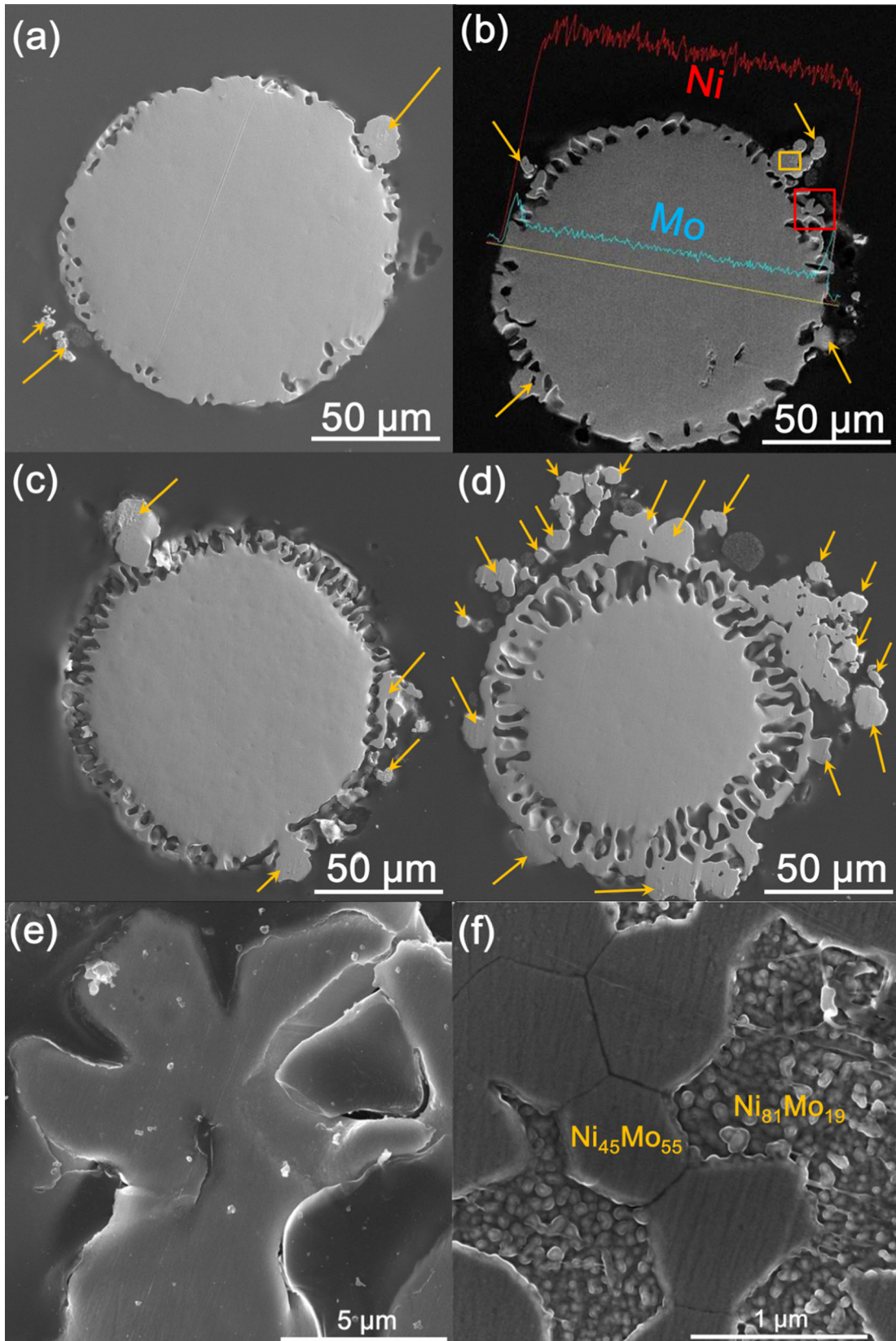


Fig. 1—Series of SEM micrographs of (a) through (d) cross-sectional views of Ni wires subjected to 2, 4, 8, and 24 h of Mo pack cementation, respectively, showing radially growing Kirkendall pores and surface protuberances (indicated by yellow arrows and sometimes appearing unconnected to wire, due to 2D-nature of cross-section); (b) shows an elemental line scan with Ni (red) and Mo (blue) concentration profiles; (e) is an enlarged view of the region shown by the red inset in (b) illustrating a surface protuberances with  $\alpha$ -Ni(Mo) composition, and (f) is an enlarged view of the region in the yellow square in (b) showing that NiMo and Ni<sub>4</sub>Mo intermetallic phases can also be formed (Color figure online).

interspacing ( $<10\ \mu\text{m}$ ) between neighboring elongated pores. It is, however, possible that tensile hoop stress generated during Kirkendall vacancy flux may assist the development of elongated pores along the subset of grain boundaries which are radially oriented,<sup>[30,31]</sup> but this hypothesis will need to be tested by further experiments where grain sizes, aspect ratios, and orientations are systematically changed.

Careful observation and measurement reveal that none of the wires experienced macroscopic distortion or significant expansion in diameter (excluding the protruding regions), although the Mo addition and the pore creation are both expected to somewhat increase the wire diameter.

### B. Protuberance Growth

As illustrated in Figures 1(a) through (d), protuberances nucleate and grow continuously on the wire surface during the pack cementation process. This phenomenon has not been documented so far among systems processed by the pack cementation technique, to our knowledge.

Two areas selected from Figure 1(b) are shown at higher magnifications in Figures 1(e) and (f), respectively. In Figure 1(e), protuberances are shown to branch and EDS analysis reveals these branches to be  $\alpha$ -Ni(Mo) solid solution with Mo contents ranging from 4 to 9 at. pct. Figure 1(f), showing the inner core of the neighboring protuberance, illustrates that it consists of a mixture of phases, identified by EDS as intermetallic phases of NiMo ( $\text{Ni}_{45}\text{Mo}_{55}$ ) and  $\text{Ni}_4\text{Mo}$  ( $\text{Ni}_{81}\text{Mo}_{19}$ ). The formation of the above phases is consistent with both literature reports<sup>[1,5,7-9,26-32]</sup> and phase diagram predictions,<sup>[33]</sup> from which the three distinct line compounds—NiMo,  $\text{Ni}_3\text{Mo}$ , and  $\text{Ni}_4\text{Mo}$ —are listed.

### C. Surface Structures

In addition to the cross-sectional observations, Ni wire surfaces were also examined to examine the morphological evolution of Kirkendall pores and protuberances, as shown in Figures 2(a) through (d). Wire surfaces roughen as the number density of protuberances (denoted by P) increases with deposition time, which is in accordance with cross-sectional examinations. In addition, the sizes of the protuberance in Figures 2(a) through (d) are consistent with those shown in cross-sections in Figures 1(a) through (d). Moreover, it appears that surface diffusion is too slow to achieve a complete smoothing of the surface protuberances, and volume diffusion to sinter surface pores.

Figures 2(a) through (d) show that the density of surface Kirkendall pores (marked as K) decreases as vapor-phase deposition continues, which could be due to the progressive growth of a Mo-rich surface layer that buries the elongated Kirkendall pores. As a consequence, pore-free surface regions gradually become dominant. Surface pores exhibit various sizes and morphologies, in particular arrays (shown in Figure 2(e)) and interlocking network structures (in Figure 2(f)), which are markedly different from those shown by

the volume Kirkendall pores, demonstrating much larger sizes and directional growth. Surface morphology features discussed above share similarities with those encountered during interdiffusion of Ni and Mn as well as Ni and Ga, leading to the creation of Ni-Mn-Ga tubes.<sup>[34]</sup>

Typical morphologies of individual protuberances are shown in Figure 3. Varying in size and shape, protuberances exhibit terraced (Figure 3(a)), rugged (Figures 3(b) and (c)), smooth (Figure 3(d)), and faceted surfaces (Figures 3(e) and (f)). They can be composed of single (Figures 3(d) through (f)) or multiple grains (Figures 3(b) and (c)) and their sides can be tapered. EDS analysis indicates these protuberances are  $\alpha$ -Ni(Mo) solid solution with approximately 9 at. pct Mo, which is consistent with findings in Figure 1(e). The Mo content in the protuberances is thus higher than that of the wire surfaces (4 at. pct). Nevertheless, we do not exclude the possibility that high Mo-containing intermetallic phases, captured in Figure 1(f), are embedded within the protuberances.

The simultaneous presence of Mo-alloyed tips, high vapor fluxes, and activated metallic elements, suggests that protuberances, analogous to nanowires grown in various systems, may be formed by the VLS or VSS mechanism.<sup>[19,21,23-25,35-38]</sup> Since the eutectic temperature of Ni-Mo binary system is 1323 °C,<sup>[33]</sup> markedly above the processing temperature of 1273 K (1000 °C), and since there are no other substances in liquid form available that could function as effective catalyst, the VLS option can be eliminated, leaving VSS as the active mechanism for the growth of protuberance. Additional features, such as faceted tips and tapered sides, also support the VSS growth mode, as emphasized by previous studies.<sup>[23-25,36,37]</sup> Although mentioned by other researchers, the possibility concerning the size effect on the melting temperature depression is not applicable to our case because all protuberances have tip sizes far exceeding the size threshold ( $<100\ \text{nm}$ ).<sup>[19,20,25]</sup>

Further compelling evidence for the operation of VSS is the presence of surface terraces and steps in sizeable quantities. As shown in Figures 3(a), (b), (d) and (f), protuberance growth is generally accompanied by the occurrence of terraces and steps. Moreover, as illustrated in Figure 4(a), terraces and steps tend to be present on struts and protuberances in the vicinity of surface Kirkendall pores. Detailed fine structures of the terraces and steps are presented in Figure 4(b), which demonstrates terraces (width ranging from 60 to 240 nm) separated by steps and circular steps progressing to form a protuberance, whose size is much less than those visible in Figure 3. The terraced structures are analogous to the surface features observed on vapor-deposited NiAl<sup>[39]</sup> and Ni-base superalloy.<sup>[40]</sup>

Protuberance growth governed by VSS mechanism can be further substantiated by the step-flow growth model,<sup>[41]</sup> which postulates that Mo adatoms diffuse along the terrace and attach to a step from both ends of the terrace. Eventually, the propagation of the steps leads to protuberance growth, which may likely serve a two-fold purpose. First, protuberance growth on the interlocking structures (Figure 4(a)) could fill the pores

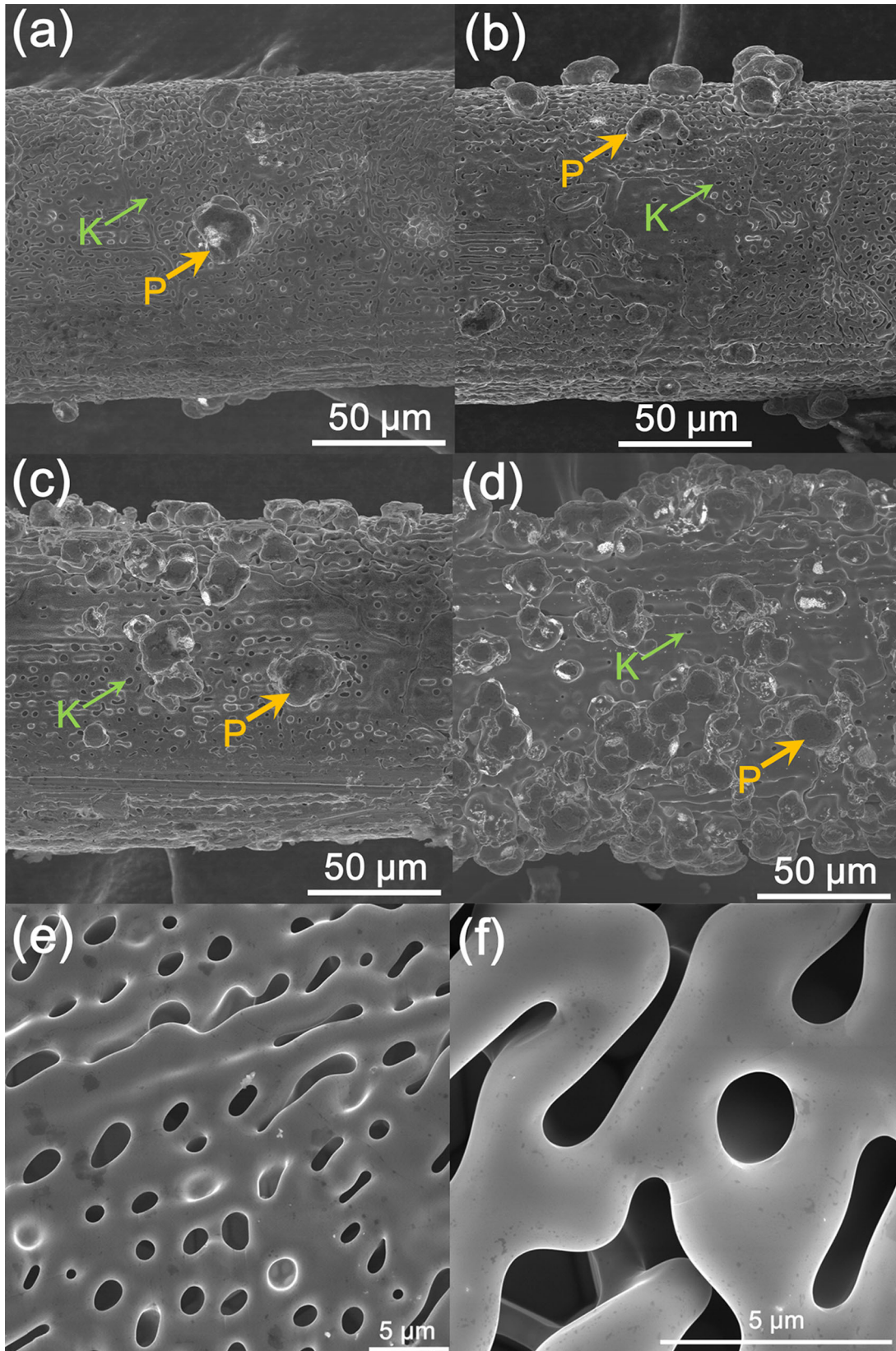


Fig. 2—SEM micrographs showing (a) through (d) surface morphology of Ni wires subjected to 2, 4, 8, and 24 h of Mo pack cementation, respectively. Labels show surface Kirkendall pores (K paired with thin green arrows) and protuberances (P paired with thick gold arrows); only one representative example, among many, is shown for each feature in each figure. Number density of surface protuberances increases while that of surface pores diminishes with increasing cementation time. (e), (f), Ni wire surface features of surface pore arrays and network structures after 2-h pack cementation (Color figure online).

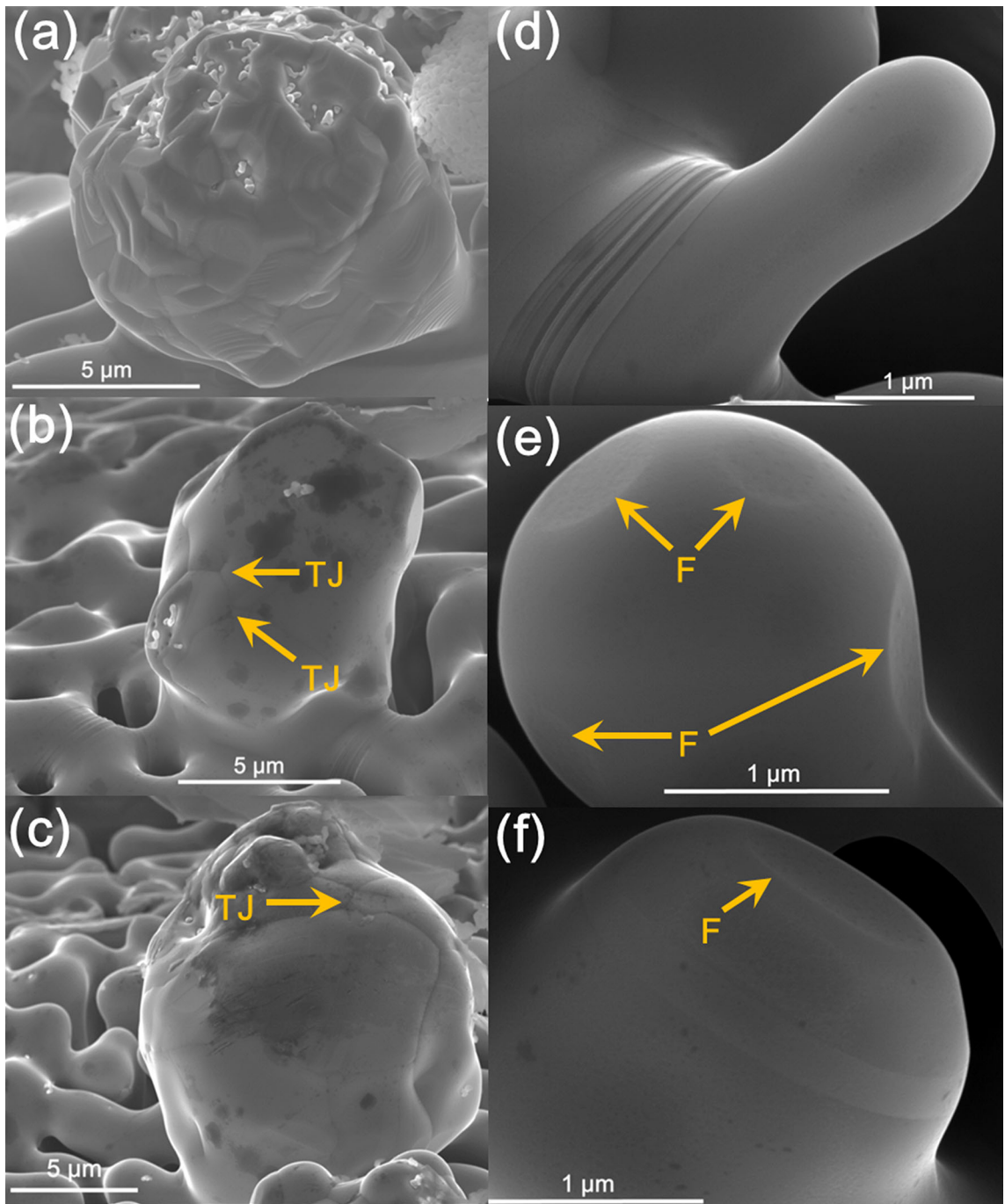


Fig. 3—Representative SEM images of (a) large-size protuberances demonstrating surface terraces and steps (white clusters are alumina powders remaining from the pack); (b) through (c) large-size protuberances demonstrating irregular surface without terraces and steps. Grain boundary triple junctions are denoted as TJ; (d) small-size protuberance showing a globular tip and a terraced tail; (e), (f) small-size protuberances showing faceted tips and sides. Facets are denoted as F. The wires were subjected to Mo pack cementation for (a) 4 h and (b) through (f) 2 h.

in their vicinity, possibly explaining the decrease in surface Kirkendall pore density shown in Figures 2(a) through (d). Second, protuberance growth on preferential surface protuberances may simply drive them to expand without any constraints. Furthermore, it is reasonable to postulate that Mo adatoms would diffuse into Ni, promoting the formation of Ni-Mo alloy in

solid form. At first, the  $\alpha$ -Ni(Mo) solid solution is produced, as confirmed by the EDS analysis on wire surfaces and protuberances. With continuing supply of Mo and its accumulation on the surface,  $\alpha$ -Ni(Mo) may become supersaturated, promoting the formation of intermetallic phase such as NiMo or Ni<sub>4</sub>Mo, as shown in Figure 1. The formation of intermetallic phases,

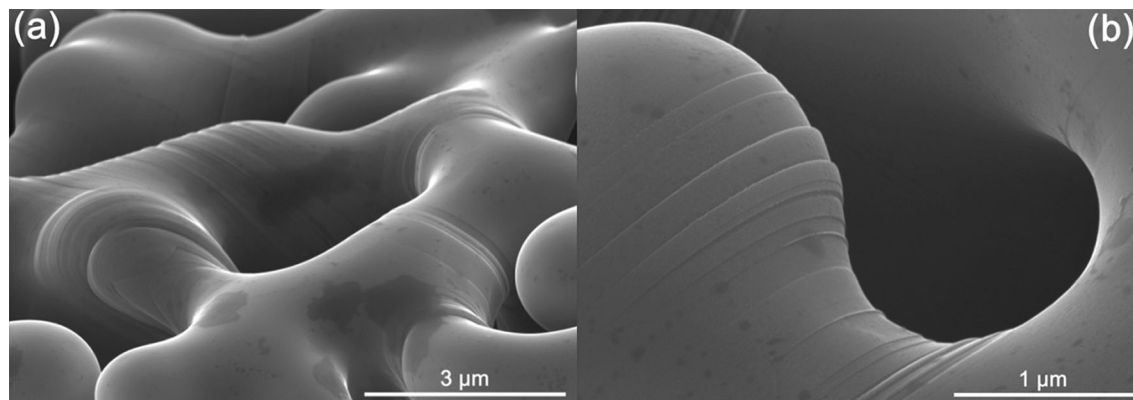


Fig. 4—Representative SEM images of (a) terraces and steps present on struts surrounding surface pores, and (b) fine structures of terraces and steps on protuberance. Wire was subjected to Mo deposition for 2 h.

according to prior investigations, could significantly accelerate the VSS process.<sup>[21–25,38]</sup> Additionally, Kirkendall pores, which reduce the interdiffusion fluxes of Mo and Ni, could enhance the outward growth of Mo-rich protuberances.

Since the pack cementation technique is widely employed, because of its simplicity, reliability and low cost, in creating coatings on Ni-base superalloys, the concurrent operation of Kirkendall effect and the VSS mechanism in the present pack cementation deposition of Mo onto Ni is of engineering significance: the pores and protuberances create notches that weaken the wires, but also increase their surface area and thus their heat exchange capacity as well as catalytic area (bare or as substrate).

#### IV. SUMMARY

The Kirkendall and VSS mechanisms are occurring concurrently during Mo vapor-phase deposition onto Ni wires and Ni-Mo interdiffusion, leading to extreme roughening of the wire surface by creation of elongated pores and protuberances. Strong imbalance in interdiffusional fluxes of Mo and Ni results in radial growth of Kirkendall pores with high aspect ratios which reduce the interdiffusion fluxes. The VSS mechanism is believed to be responsible for the growth of protuberances at the wire surface—rather than the more common vapor-liquid-solid (VLS) mechanism—as the processing temperature is considerably lower than the eutectic temperature and as protuberances exhibit distinct solid-state features, including terraces, steps, and faceted tip. The VSS process may be catalyzed by the formation of Mo-rich phases in the protuberances, such as  $\alpha$ -Ni(Mo) solid solution, and NiMo and Ni<sub>4</sub>Mo intermetallic phases. The combination of Kirkendall effect and VSS during vapor-phase deposition of Mo onto Ni roughens very substantially the surface of the wires, which may be desirable (e.g., to increase surface/volume ratio) or undesirable (e.g., because notches weaken the wire) for Mo-containing coatings on Ni-base superalloys, depending on their applications (e.g., heat exchange or structural).

#### ACKNOWLEDGMENTS

We acknowledge funding by DARPA under award number W91CRB1010004 with Dr. Judah Goldwasser as grant monitor. We thank Dr. Dinc Erdeniz and Ms. Ashley Paz y Puente (both of Northwestern University) for useful discussions, and Dr. Dinc Erdeniz for metallographic preparation of the as-received wire.

#### REFERENCES

1. C.R. Brooks, J.E. Spruiell, and E.E. Stansbury: *Int. Met. Rev.*, 1984, vol. 29, pp. 210–48.
2. W.T. Loomis, J.W. Freeman, and D.L. Sponseller: *Metall. Trans.*, 1972, vol. 3, pp. 989–1000.
3. R.A. Mackay and M.V. Nathal: *Acta Metall. Mater.*, 1990, vol. 38, pp. 993–1005.
4. H.M. Tawancy: *J. Mater. Sci.*, 1980, vol. 15, pp. 2597–2604.
5. C.P. Heijwegen and G.D. Rieck: *Acta Metall.*, 1974, vol. 22, pp. 1269–81.
6. R.D. Lanam and R.W. Heckel: *Metall. Trans. A*, 1975, vol. 6A, pp. 421–23.
7. V.D. Divya, U. Ramamurty, and A. Paul: *Metall. Mater. Trans. A*, 2012, vol. 43A, pp. 1564–77.
8. T.C. Chou and L. Link: *Scripta Mater.*, 1996, vol. 34, pp. 831–38.
9. Y. Shueh, J.P. Hirth, and R.A. Rapp: *Metall. Trans. A*, 1991, vol. 22A, pp. 1501–10.
10. M.S.A. Karunaratne and R.C. Reed: *Defect Diffus. Forum*, 2005, vols. 237–240, pp. 420–25.
11. R. Mévrel, C. Duret, and R. Pichoir: *Mater. Sci. Technol.*, 1986, vol. 2, pp. 201–06.
12. R. Bianco and R.A. Rapp: in *Metallurgical and Ceramic Protective Coatings*, K.H. Stern, Chapman and Hall, London, 1996, pp. 236–60.
13. D.C. Dunand, A.M. Hodge, and C. Schuh: *Mater. Sci. Technol.*, 2002, vol. 18, pp. 326–32.
14. C. Hounginou, S. Chevalier, and J.P. Larpin: *Appl. Surf. Sci.*, 2004, vol. 236, pp. 256–69.
15. J. Li, C. Xia, and Y. Gu: *J. Cent. South Univ.*, 2004, vol. 11, pp. 15–18.
16. R.S. Wagner and W.C. Ellis: *Trans. AIME*, 1965, vol. 233, pp. 1053–64.
17. H. Wang, L.A. Zepeda-Ruiz, G.H. Gilmer, and M. Upmanyu: *Nat. Commun.*, 2013, vol. 4, p. 1956.
18. B.J. Kim, J. Tersoff, S. Kodambaka, M.C. Reuter, E.A. Stach, and F.M. Ross: *Science*, 2008, vol. 322, pp. 1070–73.
19. S. Kodambaka, J. Tersoff, M.C. Reuter, and F.M. Ross: *Science*, 2007, vol. 316, pp. 729–32.
20. E.J. Schwalbach and P.W. Voorhees: *Nano Lett.*, 2008, vol. 8, pp. 3739–45.

21. Y. Wang, V. Schmidt, S. Senz, and U. Gosele: *Nat. Nanotechnol.*, 2006, vol. 1, pp. 186–89.
22. J. Arbiol, B. Kalache, P.R. Cabarrocas, J.R. Morante, and A.F. Morral: *Nanotechnology*, 2007, vol. 18, p. 305606.
23. Y. Yao and S. Fan: *Mater. Lett.*, 2007, vol. 61, pp. 177–81.
24. C.Y. Wen, R.C. Reuter, J. Tersoff, E.A. Stach, and F.M. Ross: *Nano Lett.*, 2010, vol. 10, pp. 514–19.
25. S.L. Wang, Y.H. He, J. Zou, Y. Wang, H. Huang, B.Y. Huang, C.T. Liu, and P.K. Liaw: *Nanotechnology*, 2008, vol. 19, p. 345604.
26. D. Erdeniz and D.C. Dunand: *Intermetallics*, 2014, vol. 50, pp. 43–53.
27. T.C. Chou and T.G. Nieh: *Thin Solid Films*, 1992, vol. 219, pp. 52–62.
28. J. Sommer, Y.M. Chiang, and R.W. Balhffi: *Scripta Metall. Mater.*, 1995, vol. 33, pp. 7–12.
29. E. Rabkin, L. Klinger, T. Izyumova, and V.N. Semenov: *Scripta Mater.*, 2000, vol. 42, pp. 1031–37.
30. L. Klinger and E. Rabkin: *Acta Mater.*, 2011, vol. 59, pp. 1389–99.
31. T. Chuang and J.R. Rice: *Acta Metall.*, 1975, vol. 21, pp. 1625–28.
32. A. Cohen, I.E. Klein, and Y.E. Yaniv: *J. Mater. Sci. Lett.*, 1985, vol. 4, pp. 1198–1202.
33. <http://www.nims.go.jp/cmssc/pst/database/mo-elem/moni/moni.htm>, Accessed 19 Sept 2014.
34. P. Zheng, P. Lindquist, B. Yuan, P. Müllner, and D.C. Dunand: *Intermetallics*, 2014, vol. 49, pp. 70–80.
35. E.A. Stach, P.J. Pauzauskie, T. Kuykendall, J. Goldberger, R. He, and P. Yang: *Nano Lett.*, 2003, vol. 3, pp. 867–69.
36. S. Hoffman, R. Sharma, C.T. Wirth, F. Cervantes-Sodi, C. Ducati, T. Kasama, R.E. Dunin-Borkowski, J. Drucker, P. Bennett, and J. Robertson: *Nature Mater.*, 2008, vol. 7, pp. 372–75.
37. M. Kolibal, R. Kalousek, T. Vystavel, L. Novak, and T. Sikola: *Appl. Phys. Lett.*, 2012, vol. 100, p. 203102.
38. S. Heun, B. Radha, D. Ercolani, G.U. Kulkarni, F. Rossi, V. Grillo, G. Salviati, F. Beltram, and L. Sorba: *Small*, 2010, vol. 6, pp. 1935–41.
39. Z. Yu, D.D. Hass, and H.N.G. Wadley: *Mater. Sci. Eng. A*, 2005, vol. 394, pp. 43–52.
40. D.T. Queheillalt, D.D. Hass, D.J. Sypeck, and H.N.G. Wadley: *J. Mater. Res.*, 2001, vol. 16, pp. 1028–36.
41. A.A. Golovin, S.H. Davis, and P.W. Voorhees: *J. Appl. Phys.*, 2008, vol. 104, p. 074301.